Geopolymer binders from metakaolin using sodium waterglass from waste glass and rice husk ash as alternative activators: a comparative study

Hervé K. Tchakouté [a,b*], Claus H. Rüscher [b], Sakeo Kong [a], Elie Kamseu [c,d], Cristina Leonelli [d]

[a] Laboratory of Applied Inorganic Chemistry, University of Yaounde I, Faculty of Science, Department of Inorganic Chemistry, PO. Box 812, Yaounde, Cameroon

[b] Institut für Mineralogie, Leibniz Universität Hannover, Callinstrasse 3, D-30167 Hannover, Germany

[c] Local Materials Promotion Authority, PO Box: 2396, Nkolbikok, Yaoundé, Cameroon

[d] Department of Engineering "Enzo Ferrari", Univeristy of Modena and Reggio Emilia, ViaP. Vivarelli 10, 41125 Modena, Italy

Abstract

Rice husk ash and waste glass from sources in Cameroon were used for producing sodium waterglass (NWG) solutions as alternative alkaline activators to prepare metakaolin-based geopolymer binders. The IR spectra of sodium waterglass from rice husk ash (S1) and from waste glass (S2) show the presence of the bands at 970 and 872 cm^{-1} respectively which could be attributed to Q^2 and Q^0 species respectively. This indicates that S2 is more reactive than S1. Metakaolin-based geopolymer cements (G1, G2) were obtained using freshly prepared NWG with a mass ratio NWG/MK = 0.83. The two geopolymer cements were characterized by mechanical testing, environmental scanning electron microscopy, mercury intrusion porosimetry, X-ray diffractometry, infrared spectroscopy and thermogravimetric analysis. The compressive strength values of geopolymer G2 (22.9, 27.6, 32.6, 36 and 39.7 MPa at 7, 14, 21, 28 and 56 days respectively) are higher than that of G1 (17.7, 19.1, 21.2, 29.9 and 32.8 MPa at 7, 14, 21, 28 and 56 days respectively) and the microstructure of G2 are more compact with fewer unreacted metakaolin particles. It can be concluded that sodium waterglass from waste glass and rice husk ash are suitable alternative alkaline activators for the production of metakaolin-based geopolymers. In addition, they constitute a better ecological choice when compared to commerciali sodium silicate from glass melting process.

Keywords: Rice husk ash, Waste glass, Sodium hydroxide, Sodium waterglass, Metakaolin, Geopolymer binders or cements (we should use the same term all over the manuscript, but this choice depend upon the journal).

* Corresponding author. Tel.: + 237 677979617/ 004917627699163
E-mail address: htchak@yahoo.fr/ hervetchakoute@gmail.com/ htchakoute@uy1.uninet.cm (**Hervé Kouamo Tchakouté**)

1. Introduction

Geopolymer cement is an inorganic polymer binding system that hardens at room temperature [1] (**Davidovits, 2011Missing in the reference list**). This new aluminosilicate material has been studied in depth by Joseph Davidovits starting from the 1970s. Geopolymerization involves a chemical reaction between amorphous aluminosilicate materials and alkaline metal silicate solutions (i.e. sodium waterglass) under highly alkaline conditions, yielding amorphous to semi-crystalline 3D polymeric structures consisting of siloxo-sialate bonds (Si-O-Si-O-Si-O-Al). Geopolymer is also known to be a term covering a class of synthetic aluminosilicate materials. It is a novel family of building materials, a new material for coatings and adhesives, new binders for fiber composites, waste encapsulation and new cement for concrete [2] (**Cioffi et al., 2011 2003 in the refences, please substitute this reference with: Provis JL, van Deventer JSJ, (2009) Geopolymers: Structures, Processing, Properties and Industrial Applications, Woodhead Publishing Ltd, Cambridge, UK**). Sodium

waterglass has been intensively used as an activator of aluminosilicate materials such as metakaolin, slag, fly ash, volcanic scoria and others. This has been identified as the activator which promotes the highest mechanical strength development [3] (**Wang et al., 1994**). However, the use of traditional sodium silicate increased the embodies energy and CO_2 emissions associated with these alkali-based-binders [4,5] (**Witherspoon et al., 2009; Tempest et al., 2009**), as consequence of it manufacturing process which involves the calcination of quartz sand with sodium carbonate at temperature between 1400 and 1500°C [6] (**Louise and Frank, 2013, correct names are : Turner LK, Collins FG,**). For the synthesis of sodium carbonate, energy is expended via the Solvay manufacturing process i.e. ammonia reacts with CO_2 (derived from calcined limestone) which is then introduced to brine which reacts to create sodium carbonate. These processes generate CO_2 as a decomposition product, and also lead to emissions from the fuel required to achieve the high-temperature conditions [7,8] (**Novotny et al., 1991; Fawer et al., 1999**). The total CO_2 emission during the synthesis of traditional sodium silicate estimated at 1514 Kg CO_2 emitted per Kg of sodium silicate [9] (**Duxson et al., 2007 there are two reference, which one?** Duxson P, Mallicoat?). This situation has promoted the development of alternative alkaline activators using some waste materials with a view towards increased sustainability for geopolymers preparation process.

Looking for silica and silicate source from waste materials, we have chosen rice husk ash and recycled sodalime glass also known as waste glass. Rice is one of the major food crops in the world and its production generates a great amount of waste in the world, namely rice husk. Cameroon is among of countries which produce rice in Africa. Rice is grown mainly in two agro-ecological zones, the Western Highlands (North-West and West Regions) and the Northern Region (North and Far-North Regions), but it is also found in smaller areas in the Centre, South-East and East Regions. The major rice cultivation projects in the country are in Maroua and Kousseri, in the Far North Region, and Ndop, in the North-West Region [10] (**Goufo, 2008**). The production of rice in the different Region of Cameroon generates a high amount of rice husk. Presently, having no commercial value in itself, rice husk usually ends up burned in open spaces, thus causing environmental pollution and disposal problems. In order to conserve energy and resources, efforts have been made [11 could we quote a reference that testify these efforts? Guofo 2008???] to burn the husk under controlled conditions and to use the resultant material as silica sources to produce sodium waterglass for the preparation of geopolymers.

In addition to rice husk, waste glass constitutes also a problem for solid waste disposal in several municipalities. The current practice is still to landfill most of the non-recyclable glass. Since glass is a non-biodegradable material, these landfills do not constitute an environmental solution. For this reason, there is a strong need to valorize this waste glass. Previous studies [12,13] (**Shi and Zheng, 2007; Federico and Chidiac, 2007**) have already made attempts to incorporate waste glass into concrete, with general focus on replacement of fine aggregate in traditional concrete systems. Recently, other studies have focused on waste glasses as flux to replace common fluxes such as feldspar to save energy in ceramic manufacturing process [14,15] (**Djangang, et al., 2014; Tiffo et al., 2015**),but the presence of waste glass poses always a major problem for the municipalities in Cameroon because it is abundant and available??? widespread is better. Nowadays, there is a not industry in charge of collecting, storing and reusing. Whereas, the use of recycled glass and rice husk ash as siliceous sources to produce sodium waterglass for geopolymers preparation or for other industrial application could be reduced significantly energy consumption and the amount of CO_2, NOx and other air pollutants emitted from the manufacturer commercial sodium waterglass.

The previous researches [16-20] (**Puertas and Torres-Carrasco, 2014a; Torres-Carrasco et al., 2014b; Torres-Carrasco and Puertas, 2015a; Torres-Carrasco et al., 2015b**) used waste glass to investigate the feasibility of using this silica source as potential alkaline activator for blast furnace slag and fly ash. The authors also checked the rheological behavior of these alkali activated materials and compared with the results obtained with standard Portland cements. But in their process, they used sodium carbonate to enhance the dissolution of silica from waste glass. **Tchakouté et al. (2015a, b**) [21,22] used sodium waterglass from rice husk ash as activators to produce metakaolin-based geopolymer binders. They also compared the properties of metakaolin-based geopolymer cements using commercial sodium waterglass and sodium waterglass from rice husk ash as activators. To reduce the environmental issues caused by disposal of waste glass and rice husk ash in several municipalities and agro-industries, the low-value silica rich wastes can be used to prepare sodium waterglass. None of the previous studies have compared the properties of metakaolin-based geopolymer binders using alternative alkaline activators such as sodium waterglass obtained from rice husk ash and from waste glass. Then, a comparative study of the reactivity of sodium waterglass from these both low-value silica-rich wastes as activators to replace efficiently traditional sodium waterglass during the metakaolin-based geopolymers preparation is of great interest.

The main target of the present work was to firstly investigate the possibility to reduce significantly the amount of energy and greenhouse gas during the production of geopolymer binders in order to promote building energy conservation through the construction of green building using low-value silica-rich wastes such as rice husk ash and waste glass to prepare alternative alkaline activators. And secondly to compare the structural, mechanical and microstructural properties of metakaolin-based geopolymer binders using alternative alkaline activators produced from chemically modified Si-rich precursors such as rice husk ash (RHA) and waste glass (WG). This study could increase public awareness of the problem of waste glass and benefits of recycling and does the same for the valorization of rice husk ash. The starting materials were characterized by chemical and mineralogical compositions and infrared spectroscopy. To monitor the formation of geopolymer binders, the products were characterized by XRD, IR absorption, TG analysis and compressive strength at 7, 14, 21, 28 and 56 days at room temperature. The amounts of binders in different geopolymer cements were also determined at the aforementioned aged. The microstructural properties of geopolymer binders at least 28 days were determined using Environmental Scanning Electron Microscopy (ESEM) and Mercury Intrusion Porosimetry (MIP).

2. Materials and experimental methods

2.1. Materials

Kaolin used in this work was extracted from Dibamba in the Littoral Region of Cameroon. Rice husk was collected from Ndop, Department of Ngoketundjia, Region of North-West (Cameroun). Waste glass bottles collected from garbage cans, were broken into pieces, washed and dried at 105 °C. Kaolin and the resulted pieces of waste glass were separately crushed in a ball mill with a porcelain jar and microspheres of high-grade alumina as grinding medium, then passing through a 90 mesh sieve and are denoted as Dib1 and WG respectively. The powder of kaolin was calcined in a programmable electric furnace (Nabertherm, Mod_LH 60/14) for 4 h at a heating rate of 1 °C/min at 700 °C to obtain metakaolin (MK). 500 g of rice husk was calcined at 600 °C for 2 h at a heating rate of 5 °C/min to obtain approximately 100 g of gray rice husk ash (RHA). NaOH pellets were supplied by Merck (KGaA, 64271 Darmstadt, Germany). Rice husk ash was previously studied by **Tchakouté et al. (2015a, b**) [21,22] and the chemical composition was shown in **Table 1**.

2.2. Experimental methods

2.2.1. Synthesis of sodium waterglass

Sodium waterglass (NWG) from rice husk ash and from waste glass were prepared by separately adding each powder of RHA and WG to sodium hydroxide pellets in order to obtain sodium waterglass with molar ratios of SiO_2/Na_2O and H_2O/Na_2O equal to 1.5 and 10, respectively. The assembly was mixed with a 200 mL of distilled water for 2 h at 100 °C using a magnetic stirrer to enhance the dissolution of silica. The solutions were subsequently filtered and the liquid were used as the activators. This procedure was described by **Tchakouté et al. (2015a, b**) [21,22]. The sodium waterglass from rice husk ash and from waste glass were denoted S1 and S2, respectively. These both activators were stored at ambient temperature for at least one week before being used in order to allow a full silica dissolution and equilibration.

2.2.2. Synthesis of geopolymer binders/concretes

Geopolymer binders/concretes were prepared by adding each freshly NWG gradually to metakaolin in a mortar and mixed for 5 min, obtaining series of samples G1 and G2, which correspond to the geopolymers from S1 and S2 respectively. The NWG/MK mass ratio was kept constant at 0.83 obtaining a suitable workability for G1 and G2. The fresh geopolymer paste samples were rapidly molded into cylindrical PE-containers (20 mm in diameter and 40 mm in height), which were closed in order to hinder water evaporation . The samples were demoulded after 24 h and sealed in the plastic for 7, 14, 21, 28 and 56 days prior to measure the compressive strength.

2.2.3. Characterization of raw materials and geopolymers

The chemical compositions of kaolin (Dib1) and waste glass (WG) were determined by X-ray fluorescence (XRF) using PANalytical Axios mAX. Thermogravimetric Analysis (TGA) of crushed geopolymer binders were performed using alumina crucible between 25-1000 °C (technical air with flow 20 ml/min, 10°C/min heating/cooling rate, Setaram Setsys Evolution 1650). X-ray diffraction (XRD) patterns were taken using CuKα radiation between 5 and 80° in 7 h in steps of 0.03° (Bruker D4). Infrared (IR) absorption spectra were taken by the KBr method (200 mg KBr, 1 mg sample, Bruker Vertex 80v, 2 cm^{-1}, 32 scans). To monitor the formation of chain and crosslink network in the different geopolymer binders, the specimens were analysed by XRD, IR absorption, TG analysis and compressive strength after 7, 14, 21, 28 and 56 days of aging at room temperature. The microstructural properties were determined by ESEM and MIP (see hereunder).

The compressive strength of the geopolymers was measured after 7, 14, 21, 28 and 56 days at room temperature using an electro-hydraulic press (Enerpac). PLEASE INDICATE HOW MANY SPECIMENS PER EACH COMPOSITION WERE TESTED AND HOW THE RESULTS ARE PRESENTED (MEAN VALUE?). The specimens were subjected to a compressive force until the specimen failed method. Before compressive strength test, each specimen was polished with sand paper to obtain flat and parallel surfaces to avoid non-uniform loading. Six samples were tested for each measurement and the mean values for the closest five were determined. After compressive strength, the fragments of each geopolymer are crushed and the obtained powders were used to measure XRD, infrared spectroscopy and TG analysis. Pieces from the mechanical testing, after gold coating and drying, were used for microstructure observations. using a JEOL JSM-6500F Environmental Scanning Electron Microscope, ESEM, with an acceleration voltage of 20.0 kV. . Pieces collected from the mechanical test were used to prepare specimens of ~ 1 cm^3 of volume for the Mercury Intrusion Porosimetry

(MIP) tests using Autopore IV 9500, 33000 psia (228 MPa) MIP covering the pore diameter range from approximately 20 to 0.001µm having two low-pressure ports and one high-pressure chamber.

To monitor the formation of uncondensed and condensed silica in each sodium waterglass, IR spectra of sodium waterglass S1, S2 were measured on a Bruker IFS66v Fourier transform spectrophotometer using the attenuated total reflection (ATR) method. The IR spectra were recorded over a range of 600-2000 cm^{-1} at a resolution 2 cm^{-1} with 30 scans.

3. Results and discussion

3.1. Characterization of starting materials

The results of chemical composition of kaolin Dib1 show high SiO_2 plus Al_2O_3 contents, 81.9 wt% in total (**Table 1**),Other oxides (Fe_2O_3, TiO_2, K_2O, P_2O_5, MgO, etc.) sum up to 5.14 %. The amount of TiO_2 indicates the presence of anatase or rutile and the presence of the lower amount of K_2O indicates the presence of the trace of micaceous, illite, or K-feldspars mineral. The presence of P_2O_5 and MgO could be attributed to the impurities of aluminosilicate phases. **Table 1** shows also the chemical compositions of RHA and WG. RHA and WG are the silica sources with content 83.05 and 68.70 wt% of silica essentially amorphous, respectively. This indicates that RHA contains a higher amount of amorphous silica. In addition to aluminum, sodium, potassium, calcium, iron, magnesium that are common oxide to these silica sources, RHA also contains manganese, phosphate and sulphur oxide as impurities.

The diffractogramm of metakaolin shows the x-ray amorphous phase with quartz, anatase and illite as crystalline impurities and shows also the typical broad hump in the range between 2θ = 18 and 35° centered around 22° (**Fig. 1**). The x-ray patterns of rice hush ash (RHA) and waste glass (WG) show a typical broad hump diffraction peak in the range between 2θ = 12 and 38° with a maximum around 22° and 29° respectively (**Fig. 2**). The higher maximum peak of WG implies the presence of high amount of amorphous phases in waste glass in the form of SiO_2, CaO, Al_2O_3 and Fe_2O_3. Besides these amorphous phases, a few crystalline peaks of quartz and many other impurities in RHA and WG can be observed,.

Fig. 3 shows the IR spectra of RHA and WG. The absorption bands at 1097, 1037, 802 and 774 cm^{-1} on the IR spectra of RHA and WG are assigned to the O-Si-O in the SiO_4 tetrahedron and the band at 466 cm^{-1} is ascribed to the bending vibration of Si-O-Si. The absorption bands at 885, 650 and 585 cm^{-1} are observed only on the IR spectra of rice husk ash (RHA) correspond to the Si-OH and/or Al-OH, Si-O or Al-O and Al-O symmetric stretching vibration and Al-O vibrations respectively. The position of the main Si–O–Si stretching band (1097 and 1037 cm^{-1} for RHA and WG respectively) gives an indication of the length and angle of the bonds in a silicate network [23] (Autef A,). According to [24] **Rees et al. (2007**), this peak occurs at approximately 1100 cm^{-1} and indicates the presence of amorphous silica. The lower wavenumber of this band for WG indicates a lengthening of the Si–O–Si bond, a reduction in the bond angle and thus a decrease of the molecular vibrational force constant [25] (**Innocenzi, 2003**).

Fig. 4 presents the IR spectrum of metakaolin (MK) and indicates the lowest absorption band at 1620 cm^{-1} is attributed to the O-H stretching and the bending vibrations of water molecules bound. The peak at 1080 cm^{-1} was assigned with asymmetric Si-O-Al and Si-O-Si. The Si-O observed at 797, 694 and 458 cm^{-1} also indicates the presence of quartz [1?, 26-29] (**Davidovits, 1991 stil missing in the reference list; Kakali et al., 2001 missing; Nayak and Singh, 2007 missing; Vizcayno et al., 2010 missing; Tchakouté et al., 2015c**). The

absorption band at 540 cm^{-1} could be related to the presence of Al-O vibrations of Al in six fold coordination, probably due to the presence of illite [29] (**Tchakouté et al., 2015c**).

Fig. 5 shows the IR spectra of sodium waterglass from rice husk ash (S1) and from waste glass (S2). The absorption bands at 872 and 970 cm^{-1} in the ATR-IR spectra of S2 and S1 could represent the ratio Q^0 and Q^2 connected $[SiO4]^{4-}$ tetrahedral respectively (**Dimas et al., 2009; Gaggiano et al., 2013**). The band at 872 cm^{-1} on the IR spectrum of S2 is attributed to Si-O-Na which silicon sites with three non-bridging oxygen (NBO) per SiO_4 tetrahedron (**Langille et al., 1991; Gaggiano et al., 2013; Autef et al., 2013; Gharzouni et al., 2015 and 2014**). The main difference between these two solutions was the presence of Q^0 species in the solution S2 indicating that S2 contains more amount of NBO. According to **Dimas et al. (2009**) and [23] **Autef et al. (2013)**, the Q^0 species are more reactive than any other Q^n, resulting in a sodium waterglass from waste glass (S2) with a higher reactivity than that of sodium waterglass from rice husk ash (S1). This indicates that S2 contained more uncondensed silica Q^0 and NB0 than that of S1 suggesting thus S2 being more depolymerized.

3.2. Characterization of geopolymer binders

3.2.1. Mechanical and microstructural properties

Fig. 6 shows the compressive strength of metakaolin-based geopolymer binders G1 and G2 at various curing time (between 7 and 56 days). The results show that the strength of geopolymer binders increased with the curing time from 17.7 to 32.8 MPa for G1 and from 22.9 to 39.7 MPa for G2 (are these data accompained by an error or a standard deviation???). This trend indicates that the polycondensation process improves when the curing time increase. Significant differences were noted in the compressive strength development of the geopolymer binders using sodium waterglass from raw rice husk ash and waste glass. The figure shows that the maximum compressive strength was obtained using sodium waterglass from waste glass (39.7 MPa at 56 days). This indicates that S2 generates higher amounts of NBO atoms which enhances the formation of Q^0 (peak at 872 cm^{-1} in **Fig. 5**) species. This caused the dissolution of considerable metakaolin and subsequent gradual shift of the chemical system from the monosilicate chains and cyclic trimers to species with larger rings and complex structures and polymers, resulting in the 3D polymeric framework and increasing the compressive strength of geopolymer binders G2. The presence of Ca-ions in sodium waterglass from waste glass (S2) involved the chemical reaction between Ca^{++} ions and aluminate, silicate species. This reaction continues until all available Ca^{++} ions are exhausted and with time, concentration of Ca^{++} ions becomes the limiting factor for this reaction (**Chindaprasirt et al., 2012**). The pH of the system also decreased with time, due to the consumption of OH^- during hydrolysis to form further silicate and aluminate species. This confirmed why the value of the main band of G2 between 7 and 14 days increased from 1000 to 1006 cm^{-1} (see below in **Fig. 12**). The low pH and limited Ca^{++} ions environments promote the polymerization reaction between silicate and aluminate species producing more geopolymer gels (**Chindaprasirt et al., 2012**) in G2. Whereas IR spectrum show the peak at 970 cm^{-1} which indicates the formation of Q^2 in S1 (**Dimas et al., 2009**; **Autef et al., 2013**) suggesting thus S1 contained a condensed silica and less amount of NBO which hinders the dissolution of metakaolin and entails the lower compressive strength (32.8 MPa at 56 days). The values of the mechanical strength of the metakaolin-based geopolymer binders using S1, compared with the one observed in geopolymers activated with S2, is likely to be determined by the different rates of release of silicate in these systems in the early stages of geopolymerization. This influences directly the structural characteristics of the binders and consequently their compressive strengths

(**Criado et al., 2007; Hajimohammadi et al., 2011**). In geopolymers activated with S1, it was expected that there would have benn lower dissolved silica content in the solutions compared with S2 (as confirmed by IR spectra of S1), as a consequence of partial dissolution of some amorphous phases present in the RHA, during at least one week allowed for the equilibration of the solutions. The presence of these remnants partially dissolved silica particles would be expected to slow down the availability of SiO_2 in the system, leading to a slightly lower compressive strength development of metakaolin-based geopolymer G1. Consequently, higher reactive silica content in S2 induces the formation of high aluminosilicate gel content in G2 and, with it, high mechanical strength.

Fig. 7 shows the ESEM images of the metakaolin-based geopolymer binders G1 (G1a, b and c) and G2 (G2d, e and f). The micrographs reveal that the specimens using sodium waterglass from rice husk ash (G1) were heterogeneous due to the less dissolution of metakaolin (G1a). Considerable unreacted metakaolin are clearly observed in G1 as discussed below. The unreacted metakaolin in G1 settles to the geopolymer gels but not connected to the network. This could be related to the presence of condensed silica in S1, represented by species Q^2 (**see Fig. 5**), which hinders the depolymerization of metakaolin. Whereas the micrographs of G2 show a homogeneous material, more compact with fewer unreacted metakaolin and certain large particles and pores were overlapping in the matrix (G2d, e and f). This microstructural features are due to the higher reactivity of S2. The micrographs of G1b and G2e present relatively coarse microstructures but G2e has a more enhanced connectivity between the grains and polysialate particles due to the greater depolymerization of metakaolin. This greater connectivity and the size of polysialate formed during the polycondensation process will (??) increase the cross linking between grains and polysialate particles of G2 (**Duxson et al., 2005; Duxson et al., 2007; Kamseu et al., 2011**) suggesting thus higher strength. At higher magnification (2000x) the denser matrices and strong connectivity of gel for G2 compare to G1 (see **Fig. 7** G1c, G2f) are visible. The presence of Ca-ions in the structure of G2 promotes the formation of highly densified structure and consequently enhanced the compressive strength (**Bernal et al., 2012**).

The MIP technique provides a better understanding of the effects of both alkaline solutions S1, S2 on the connectivity and extension of the pore structure in geopolymer binders G1 and G2. **Fig. 8** shows the cumulative pore volume and average pore radius of G1 and G2. It can be seen that the cumulative pore volume and average pore radius of G1 are 275 mm^3/g and 17 nm, respectively, while those of G2 are 245 mm^3/g and 50 nm, respectively. According to **Sing et al. (1985)**, pores of widths between 2 and 50 nm are called mesopores. This indicates that the pores observed in geopolymer binders G1 and G2 have the aperture range of the mesopores. It is important to note that the cumulative pore volume of G2 is lower than the one of G1 but the average pore radius is higher than the one of G1. The higher average pore radius in G2 could be related mainly to the more replacement of Si by Al during the depolymerization of the metakaolin which decreases the ratio Si/Al and increase the negative charge in the aluminosilicate gel using S2 as an activator as discussed below (IR spectra). But the presence of Ca-ions in sodium waterglass (S2) come within mesopores of geopolymer gel and contributed to the protection of Al–O–Si bonds within the aluminosilicate network (**Rüscher et al., 2011**) suggesting thus higher compressive strength (**see Fig. 6**) as discussed below (IR spectra section).

3.2.2. Mineralogical characterization

The XRD patterns of G1 and G2 as function of curing time show the typical broad peak structure centered around 28° 2Theta using CuKα radiation (**Figs. 9 and 10**). A shoulder in this peak structure with higher

intensity on the x-ray patterns of G1 could be seen at between 21 and 27° 2Theta (this band is nearly similar to the one of metakaolin (**Fig. 1**)), which could indicate the presence of more unreacted metakaolin particles as discussed below. This shoulder band decreases with increasing the aging and entails that the polycondensation process increases with the time suggesting thus the development of compressive. Whereas the intensity of this peak is lower on the x-ray patterns of G2. This could be related mainly to the more depolymerization of metakaolin and the formation of longer poly(sialate-siloxo) chains in G2 compared to G1. This confirms that sodium waterglass from waste glass is more reactive than the one from rice husk ash using metakaolin as aluminosilicate material suggesting thus G2 is more compact and have a higher compressive strength (**see Figs. 6 and 7**). Moreover, the additional mineral phases such as quartz, anatase and illite are clearly observed also on the XRD patterns of geopolymer cements as they were detected in the metakaolin. This implies that these minerals remained unaltered. We expected the presence of CASH (calcium aluminosilicate hydrate) gel in G2 due to the presence of Ca^{++} ions in the gel, but according to **Chindaprasirt et al. (2012**), the CASH gel is stable at high pH (> 12) environments whilst NASH (sodium aluminosilicate hydrate) gel is stable at lower pH (9-12). The presence of Ca^{++} ions in the system decreased the pH and promotes the formation of NASH gel which is mainly responsible for the strength development. This explains the absence of the CASH gel on the XRD patterns of G2.

3.2.3. Infrared spectroscopy

Figs. 11 and 12 display the IR spectra of metakaolin-based geopolymer binders G1 and G2 at different curing time. In the IR spectra of G1 and G2, bands between 1380 and 1656 cm^{-1} are associated with OH vibrations, which are characteristic of weak H_2O molecules that have been either surface absorbed or caught in the structure cavities (**Heah et al., 2012**). The band between 443 and 452 cm^{-1} are attributed to Si-O-Si in plane bending vibration. The absorption band at 694 cm^{-1} is ascribed to Si-O symmetric stretching vibration and the bands around 718-720 cm^{-1} are assigned to Si-O-Al bending vibration, indicating that main geopolymer structure generated after the reaction between the silicon aluminates and the highly alkali solution was a bending Si-O-Al (**Gao et al., 2014**). According to **Lecomte et al. (2006)**, the formation of this band is ascribed to the formation of highly cross linking geopolymer gel framework. These bands are broad on the IR spectra of G1 except G1 at 56 days and sharp on the IR spectra of G2. This could be related to the more depolymerization of metakaolin in G1 at 56 days and G2 suggesting thus the polycondensation process in G1 continuous with the curing time. A weak Si-O-Al bending band with Al in six fold coordination was observed at 565 cm^{-1} only on the IR spectra of G1. This could be indicating that Al in six coordination still in G1 suggesting thus G1 contained more unreacted metakaolin and entails low compressive strength (**Fig. 6**). The absorption bands between 1024 and 1001 cm^{-1} (**see Figs. 9 and 10**) are ascribed to Si-O-Si and Si-O-Al asymmetric stretching vibration. According to **Chindaprasirt et al. (2009**), these bonds, known as the main band of geopolymers, are often used to determine the degree of polymerization because these peaks are more obvious than the Si-O-Si bonding peak. The values of the wavenumbers of these main bands are higher on the IR spectra of G1 compare to G2. This could be related to the greater dissolution of metakaolin and the higher Al inclusions in G2 (**Milkey, 1960; Rüscher et al., 2010**) suggesting thus the formation of an aluminosilicate network and could also be related to the presence of Ca-ions in sodium waterglass S2 lead to the shift of the main band of geopolymers G2 toward a lowest wavenumber, suggesting structural changes associated with enhanced polymerization of the gel (**Chindaprasirt et al., 2009**) as confirmed by the results compressive strength and ESEM observations. In these systems, the Ca-ions is believed to be associated with the Si–O–Al framework of the geopolymeric gel, contributing to balance the

negative charge associated with tetrahedral Al(III) due to the presence of more Al inclusion in the system and indicates also the rise in the tetrahedral aluminum content. With the replacement of Si^{4+} by Al^{3+}, the Si-O-Al angle became more acute, shifting the signal to lower frequencies due weaker bond and to the fact that the Al-O bond is longer than the Si-O bond. That means that the soluble Si atom content was higher in sodium waterglass from waste glass (S2) suggesting thus more depolymerization of metakaolin. The highest wavenumber of the main band of G1 (1024 -1019 cm^{-1}, see **Fig. 11**) could be related to the partial replacement of Si by Al in the gel structure. This justifies the presence of the band at 565 cm^{-1} on the IR spectra of G1. **Fig. 11** shows that with the increase the curing time, the values of the wavenumber of main band shifted to a lower frequency, which indicates that the polymerization degree strengthened. According to **Rüscher et al. (2011**), this shift is essentially related to the slow formation of an aluminosilicate network either enclosing the silicate chains or even cross-linking them. IR spectra **(Fig. 12)** show that between 7 and 14 days, the value of the wavenumber of the main band is at 1000 and 1006 cm^{-1} , respectively. The increase of these values could be related to the consumption of hydroxide from sodium waterglass (S2) due to the presence of Ca^{++} ions (as discussed above) leads to the polymerization of silicate units. For curing time longer than 14 days, a systematic shift occurs to 1001 cm^{-1} at 56 days. This can be related to the slow formation of an aluminosilicate network enclosing oligomeric units. Between 21 and 28 days, the values of the wavenumber of main band are stable. According to **Mielcarek et al. (2008**), this could be related to the further structural changes which enclose the destruction of silicate chains and the tendency to form a homogeneous aluminosilicate network. This assertion is confirmed by the result of microstructure of G2 (**see Fig. 7**) which show that the micrographs of G2 are homogeneous, compact and have the denser matrices.

3.2.4. Determination of the amount of unreacted metakaolin

Fig. 13 shows the elaborated IR spectra of the binder obtained by subtracting of around 25% of IR recorded for pure metakaolin from that of G1 at 7, 14, 21 days, 17% and 15% from that of G1 at 28 and 56 days respectively. Whereas **Fig. 14** shows similar elaboration where the IR spectra of the binder was obtained by subtracting 15%, 12%, 10%, 9% and 5% from that of G2 at 7, 14, 21, 28 and 56 days respectively. The resulting spectra show that the value of the wavenumber of the main band is the same (about 1000 cm^{-1}) indicating that the silicate gel binder molecular structure is nearly the same in G1 and G2. This elaboration suggest thus more metakaolin particles in G2 is nearly dissolved due to the lower wavenumber values with respect to the main band shown in **Fig. 12**. **Rüscher et al. (2010)** investigated the effect of compressive strength of metakaolin-based geopolymer cements between 1 and 700 h. They reported that when considerable metakaolin particles dissolved during the geopolymerization, the compressive strength values showed a strong increase between 25 and 100 h but decreased again above 200 h for aging. They concluded this could be related to the destruction of the polymeric silicate chains. Conversely, in this work the compressive strength increased with increasing the aging. This observation could be related to the presence of higher amount of Ca-ions in G2 (come from waste glass, **see Table 1**) which contributed to the protection of the long polysiloxo chains (**Rüscher et al., 2011**). It can be concluded that G1 contained considerable unreacted metakaolin particles in their structure. These results confirm the findings of the XRD patterns (**Fig. 6**) and the microstructure of geopolymer binders G1 and G2 (**Fig. 7**) which suggested that G1 contained considerable unreacted metakaolin particles. The resulting IR spectra of the binder show that the amounts of unreacted metakaolin particles decrease with increasing the curing time suggesting that the polycondensation process increases with the ageing and contributed to the formation of long

chains –Si-O-Si-O-Al-O-Si- in the network. It can be concluded that geopolymer cements G1 content approximately 75% of binder between 7 and 21 days. Such content increases up to 83% and 85 % of the binder at 28 and 56 days respectively. Whereas G2 presnets a content around 85%, 88%, 90%, 91 and 95% of binder at 7, 14, 21, 28 and 56 days respectively. These results are in good agreement with the findings of compressive strength, X-ray patterns, IR spectroscopy and microstructure.

3.2.5. Thermogravimetric analysis

TGA curves of geopolymer binders G1 and G2 with various curing time (7 to 56 days) are shown in **Fig. 15**. The major weight loss is observed at the temperature below 180 °C for G1 and G2 and indicates the removal of absorption water or free water (**Rosas-Casarez et al., 2014**). The second thermal degradation occurs between 180 and 350 °C and is specifically associated with the presence of sodium aluminosilicate gel (**Rosas-Casarez et al., 2014**). The remaining weight loss at between 350 and 650 °C can be attributed to more bound water which results from the condensation of silanol or aluminol groups (**Duxson et al., 2007**). According to **Davidovits (2011)**, this latter weight loss is due to dehydroxylation of OH groups, and subsequent polycondensation into siloxo bond Si-O-Si, linking neighboring geopolymeric micelles. The results of these curves show approximately 18.58 , 16.06 , 15.02 , 12.57 and 12.36 wt% were lost for G1 at 7, 14, 21, 28 and 56 days, respectively, while G2 at 7, 14, 21, 28 and 56 days lost about 17.36 , 16.18 , 16.08 , 15.04 and 14.78 wt%, respectively (I wonder if these values should be given with this accuracy...in TGA the values are give with two figures: 18 instead of 18.58). The mass loss decreases with increasing the curing time but its decrease slowly between 7 and 21 days (**Fig. 16**). This indicates that the dissolution process of metakaolin between 7 and 21 days is lower and this explains why the compressive strengths are a little weak these days especially for G1. Between 21 and 56 days, the depolymerization of metakaolin continues and more water participates to this process and is included in the structure of geopolymer cements. This result corroborates the result of the IR spectra of G1 and G2 which indicates more dissolution of metakaolin between 21 and 56 days (**Figs. 11 and 12**) due to the decreasing of the frequency of the main band. Between 28 and 56 days, the amount of the mass loss of G1 (12.57 wt% and 12.36 wt%) is lower compare to the one of G2 (15.04 wt% and 14.78 wt%). This suggests that between 28 and 56 days, the structure of geopolymer binders G2 contained more condensed or chemically bound water. According to **Temuujin et al. (2012)**, a more condensed geopolymers structure contain structural water in their cavities, while in a less condensed structure, water is present mostly as free water and released during hardening. The releasing of free water during the hardening induces higher value of cumulative pore volume (275 mm^3/g) in the structure of G1 as confirmed by MIP. According to **Ramadhansyah et al. (2012)**, the greater the weight loss, the higher of amorphous phase in samples indicating thus more binder in the geopolymer cements G2 (as discussed above) suggesting higher compressive strength, denser matrices, less unreacted metakaolin and less pore volumes (compare **Figs. 6, 7, 8 and 13**).

4. Conclusion

The Cameroon low-value silica-rich wastes such as rice husk ash and waste glass were used to prepare alternative alkaline activators with molar ratios SiO_2/Na_2O and H_2O/Na_2O equal to 1.5 and 10 respectively. These synthesized alkaline solutions were used to prepare metakaolin-based geopolymer binders. The mechanical properties of metakaolin-based geopolymer cements depended on the type of silica sources used to produce sodium waterglass. The geopolymer binders using sodium waterglass from waste glass exhibited a

smaller cumulative pore volume; consequently, its compressive strength was greater and the microstructure was more (?) compact with fewer unreacted metakaolin particles. The compressive strength of geopolymer binders increased with the curing time and the maximum of 39.7±??? MPa was recorded for geopolymer cements obtained using sodium waterglass from waste glass and 32.8±??? MPa for the one using sodium waterglass RHA at 56 days. The weight loss recorded for G2 was 14.78% while the one of G1 wais 12.36% suggesting thus G2 could a very suitable material for fire resistant applications. This work has proven that sodium waterglass from waste glass and rice husk ash are suitable alternative alkaline solutions for the production of metakaolin-based geopolymers and could replace sodium silicate solutions obtained from mineral sources.

Acknowledgement

Hervé Tchakouté Kouamo gratefully acknowledges the Alexander von Humboldt Foundation for financially support his Postdoctoral research (N° **KAM/1155741 STP**) in Institut für Mineralogie, Leibniz Universität Hannover, Germany.

References

Autef A, Prud'Homme E, Joussein E, Gasgnier G, Pronier S, Rossignol S. (2013) Evidence of a gel in geopolymer compounds from pure metakaolin. J Sol-Gel Sci Technol; 67: 534–44.

Bernal, S. A., Rodriguez, de Gutierrez, E.D.R. M., Provis, J.L., Delvasto, S. Activation of metakaolin/slag blends using alkaline solutions based on chemically modified silica fume and rice husk ash. Waste and Biomass Valorization (2012) 3: 99–108.

Chindaprasirt P, Jaturapitakkul C, Chalee W, Rattanasak U (2009) Comparative study on the characteristics of fly ash and bottom ash geopolymers. Waste Management; 29: 539-543.

Chindaprasirt P, De Silva P, Sagoe-Crentsil K, Hanjitsuwan S (2012) Effect of SiO_2 and Al_2O_3 on the setting and hardening of high calcium fly ash-based geopolymer systems. J Mater Sci 47: 4876–4883.

Cioffi R., Maffucci L., Santoro L. Optimization of geopolymer synthesis by calcinations and polycondensation of a kaolinitic residue. Resources, Conservation and Recycling, 40, 27–38, 2003.

Criado M, Fernandez-Jimenez A, de la Torre AG, Aranda MAG, Palomo A (2007)An XRD study of the effect of the SiO_2/Na_2O ratio on the alkali activation of fly ash. Cem. Concr. Res. 37, 671–679.

Dimas D, Giannopoulou I, Panias D. (2009) Polymerization in sodium silicate solutions: a fundamental process in geopolymerization technology. J Mater Sci 44: 3719–30.

Djangang CN, Kamseu E, Elimbi A, Lecomte GL, Blanchart P (2014) Net-shape clay ceramics with glass waste additive. Materials Sciences and Applications5(8): 592-602.

Duxson P, Mallicoat SW, Lukey GC, Kriven WM, Van Deventer JSJ. The effect of alkali and Si/Al ratio on the development of mechanical properties of metakaolin-based geopolymers. Colloids Surf A: Physicochem Eng Aspects 2007; 292(1):8–20.

Duxson P, Provis JL, Lukey GC, Mallicoat SW, Kriven WM, Van Deventer JSJ. Understanding the relationship between geopolymer composition, microstructure and mechanical properties. Colloids Surf A: Physicochem Eng Aspects 2005; 269:47–58.

Duxson, P, Provis, J.L, Lukey, G.C, van Deventer, J.S.J., 2007. The role of inorganic polymer technology in development of 'green concrete'. Cem. Concr. Res. 37: 1590–1597.

Fawer M, Concannon M, Rieber W (1999). Life cycle inventories for the production of sodium silicates. Int. J. Life Cycle Assess. 4(4), 207–212

Federico LM Chidiac SE (2009) Waste glass as a supplementary cementitious material in concrete – Critical review of treatment methods. Cement and Concrete Composites,. 31(8): 606-610.

Gaggiano R, De Graeve I, Mol JMC, Verbeken K, Kestens LAI, Terryn H (2013) An infrared spectroscopic study of sodium silicate adsorption on porous anodic alumina. Surf Interface Anal; 45: 1098-1104.

Gao K, Lin KL, Wang D, Hwang CL, Shiu HS, Chang YM, Cheng TW, (201). Effect of SiO_2/Na_2O molar ratio on mechanical properties and the microstructure of nano-SiO_2 metakaolin-based geopolymers. Constr. Build. Mater. 53: 503-510.

Gharzouni A, Joussein E, Samet B, Baklouti S, Rossignol S. (2015) Effect of the reactivity of alkaline solution and metakaolin on geopolymer formation. J Non-Cryst Solids; 410: 127–34.

Gharzouni, A., Joussein, E., Samet, B., , Sanz, J., Rossignol, S. (2014) The effect of an activation solution with siliceous species on the chemical reactivity and mechanical properties of geopolymers, J. Sol-Gel Sci. Technol. 73(1): 250-259

Goufo P, (2008)-. Rice Production in Cameroon: a Review. Res. J. Agri. Biol. Sci. 4: (6), 745-756.

Hajimohammadi A, Provis JL, van Deventer JSJ (2011)The effect of silica availability on the mechanism of geopolymerization. Cem. Concr. Res. 41(3): 210–216.

Heah CY, Kamarudin H, Mustafa Al Bakri AM, Bnhussain M, Luqman M, Khairul Nizar I et al. Study on solids-to-liquid and alkaline actvator ratios on kaolin-based geopolymers. Contruction and Building Materials 2012; 35: 912-922.

Innocenzi P.(2003) Infrared spectroscopy of sol-gel derived silica-based films: a spectra-microstructure overview. J Non-Cryst Solids; 316:309–319.

Jani, Y. and W. Hogland, Waste glass in the production of cement and concrete – A review. Journal of Environmental Chemical Engineering, 2014. 2(3): 1767-1775.

Kamseu E, Leonelli C, Chinje Melo UF, Perera D, Lemougna LN. Polysialate matrixes from Al-rich and Si-rich metakaolins: polycondensation and physico-chemical properties. Interceram 2011; 60(1): 25–31.

Langille KB, Nguyen D, Bernt JO, Veinot DE, Murthy MK. Mechanism of dehydration and intumescence of soluble silicates: Part I Effect of silica to metal oxide molar ratio. J Mater Sci 1991; 26: 695-703.

Lecomte, I., Henrist, C., Liegeois, M., Maseri, F., Rulmont, A., Cloots, R.: (Micro)-structural comparison between geopolymers, alkali-activated slag cement and Portland cement. J. Eur. Ceram. Soc. 26, 3789–3797 (2006).

., Turner LK, Collins FG, (2013) Carbon dioxide equivalent (CO_2-e) emissions: A comparison between geopolymer and OPC cement concrete. Constr. Build. Mater. 43: 125–130.

Mielcarek E, Rüscher CH. Meeting of the German crystallographic society, Erlangen, Germany 2008.

Milkey RG. Infrared spectra of some tectosilicates. Amer Mineral 1960; 45: 990-1007.

Novotny R. Hoff A, Schuertz J, (1991) Process for hydrothermal production of sodium silicate solutions. United States Patent, N° 5000933.

Puertas F, Torres-Carrasco M (2014a) Use of glass waste as an activator in the preparation of alkali-activated slag. Mechanical strength and paste characterization. Cement and Concrete Research 57: 95-104.

Ramadhansyah, P.J., Mahyun, A.W., Salwa, M.Z.M., Abu Bakar, B.H., Megat Johari, M.A., Wan Ibrahim, M.H., 2012. Thermal analysis and pozzolanic index of rice husk ash at different Grinding time. Procedia Eng. 00: 000-000.

Rees CA, Provis JL, Lukey GC, van Deventer JSJ. (2007) In situ ATR-FTIR study of the early stages of fly ash geopolymer gel formation. Langmuir; 23: 9076–9082.

Rosas-Casarez, C.A., Arredondo-Rea, S.P., Gómez-Soberón, J.M., Alamaral-Sánchez, J.L., Corral- Higuera, R., Chinchillas-Chinchillas, M.J., Acuña-Agüero, O.H., 2014. Experimental study of XRD, FTIR and TGA techniques in geopolymeric materials. Proc. of the Intl. Conf. on Advances In Civil and Structural Engineering - CSE.

Rüscher CH, Mielcarek EM, Wongpa J, Jaturapitakkul C, Jirasit F, Lohaus L (2011) Silicate-, aluminosilicate and calciumsilicate gels for building materials: chemical and mechanical properties during ageing. Eur. J. Mineral., 23, 111–124.

Rüscher CH, Mielcarek E, Lutz W, Ritzmann A, Kriven WM (2010) Weakening of alkali-activated metakaolin during aging investigated by the molybdate method and infrared absorption spectroscopy. J Am Ceram Soc; 93: 2585–2590.

Shi C,Zheng K. (2007) A review on the use of waste glasses in the production of cement and concrete. Resources, Conservation and Recycling, 52(2): p. 234-247.

Sing KSW, Everett DH, Haul RA.W, Moscou L, Pierotti RA, Rouquerol J, Siemieniewska T, (1985) Reporting physisorption data for gas/solid systems with special reference to the determination of surface area and porosity. Pure Appl. Chem. 57: 603–619.

Tchakouté HK, Rüscher CH, Kong S, Kamseu E, Leonelli C (2015b) Comparison of metakaolin-based geopolymer cements from commercial sodium waterglass and sodium waterglass from rice husk ash. Construction and Building Materials (under review).

Tchakouté HK, Rüscher CH, Kong S, Kamseu E, Leonelli C (2015a) Synthesis of sodium waterglass from rice husk ash as activator to produce metakaolin-based geopolymer binders. Journal of Cleaner Production (under review).

Tchakouté, H.K., Rüscher, C.H., Djobo, J.N.Y., Kenne, B.B.D., Njopwouo, D., 2015c. Influence of gibbsite and quartz in kaolin on the properties of metakaolin-based geopolymer cements. Appl. Clay Sci. 107: 188–194.

Tempest B, Sanusi O, Gergely J, Ogunro V, Weggel D (2009) Compressive strength and embodied energy optimization of fly ash based geopolymer concrete. In: Proceedings of the 2009 World of Coal Ash (WOCA) Conference. Lexington, KY, USA.

Temuujin, J., Minjigmaa, A., Rickard, W., van Riessen, A., 2012. Thermal properties of spray-coated geopolymer-type compositions. J. Therm. Anal. Calorim. 107: 287–292.

Tiffo E, Elimbi A. Dika Manga J. Tchamba AB (2015) Red ceramics produced from mixtures of kaolinite clay and waste glass. Braz J Sci Technol Doi:10.1186/s40552-015-0009-9..

Torres-Carrasco M, Palomo JG, Puertas F, (2014b) Sodium silicate solutions from dissolution of glass wastes. Statistical analysis. Materiales de Construccion 64 (314): 1-14.

Torres-Carrasco M, Puertas C, Mar Alonso M, Puertas F, (2015b) Alkali activated slag binders using waste glass as alternative activators, Rheological behavior. Boletín de la Sociedad Española de Cerámica y Vidrio 54(2): Doi: 10.1016/j.bsecv.2015.03.004.

Torres-Carrasco M, Puertas F, (2015a) Waste glass in the geopolymer preparation. Mechanical and microstructural characterization, Journal of Cleaner Production 90: 397-408.

Wang SD, Scrivener KL, Pratt PL (1994) Factors affecting the strength of alkali-activated slag. Cem. Concr. Res. 24(6): 1033–1043

Witherspoon R, Wang H, Aravinthan T, Omar T (2009) Energy and emissions analysis of fly ash based geopolymers. SSEE International Conference - Solutions for a Sustainable Planet. Melbourne, Victoria, Australia: Society for sustainability and environmental engineering; Paper 29..

Table 1
Chemical composition (wt%????) of kaolin (Dib1), rice husk ash (RHA) and waste glass (WG). Add comments on the error or add standard deviation

Oxide	Dib1	RHA	WG
SiO_2	54.50	83.05	68.70
Al_2O_3	27.40	1.82	1.90
Fe_2O_3	2.55	0.58	0.56
K_2O	0.28	5.65	0.75
TiO_2	2.21	0.10	<0.1
MgO	0.09	3.59	2.33
Na_2O	<0.1	0.13	12.6
CaO	0.10	0.69	14.30
SO_3	<0.02	0.34	/
P_2O_5	0.079	3.81	/
ZnO	/	0.03	/
MnO	/	0.15	<0.1
Rb_2O	/	0.03	/
SrO	/	0.003	/
ZrO_2	/	0.005	/
LOI	11.19	/	0.55

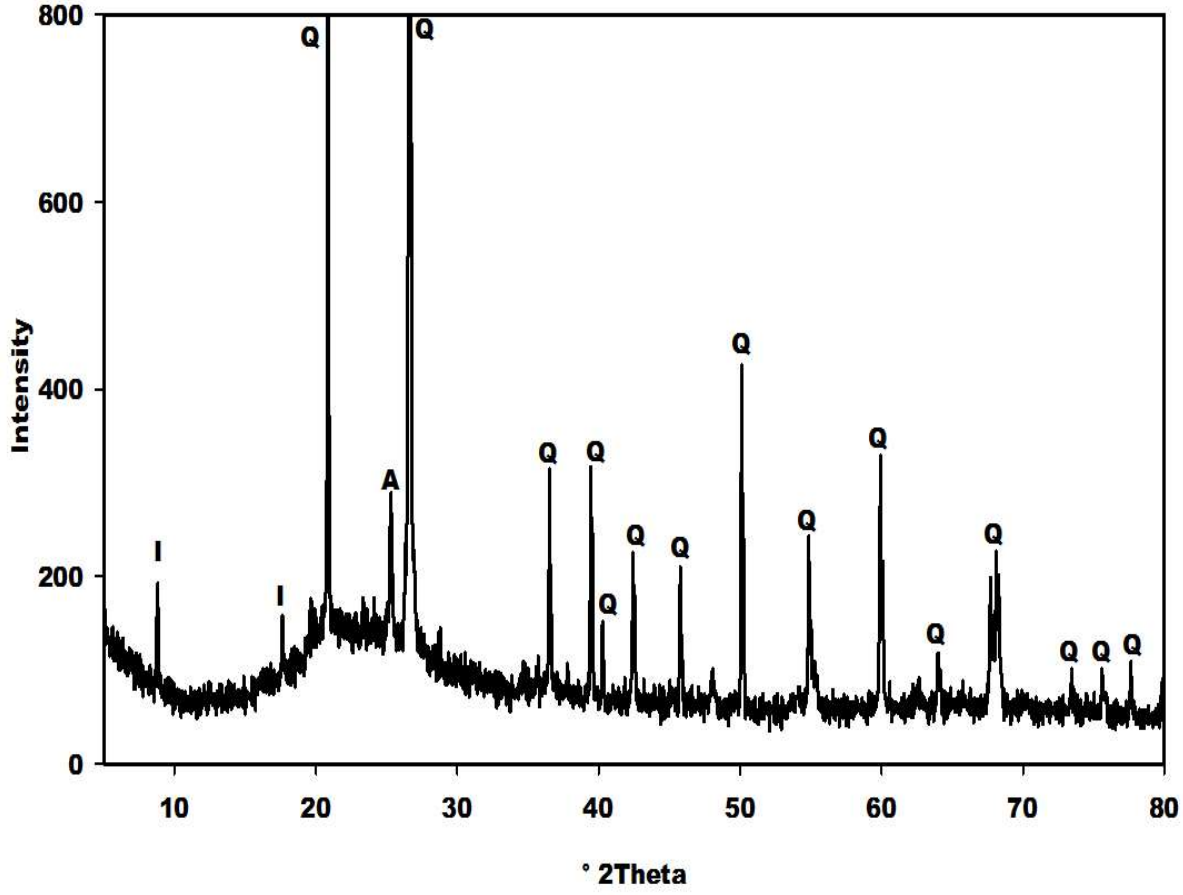

Fig.1. X-ray pattern of metakaolin, MK. (I, A and Q denote peaks of Illite, Anatase and Quartz respectively).

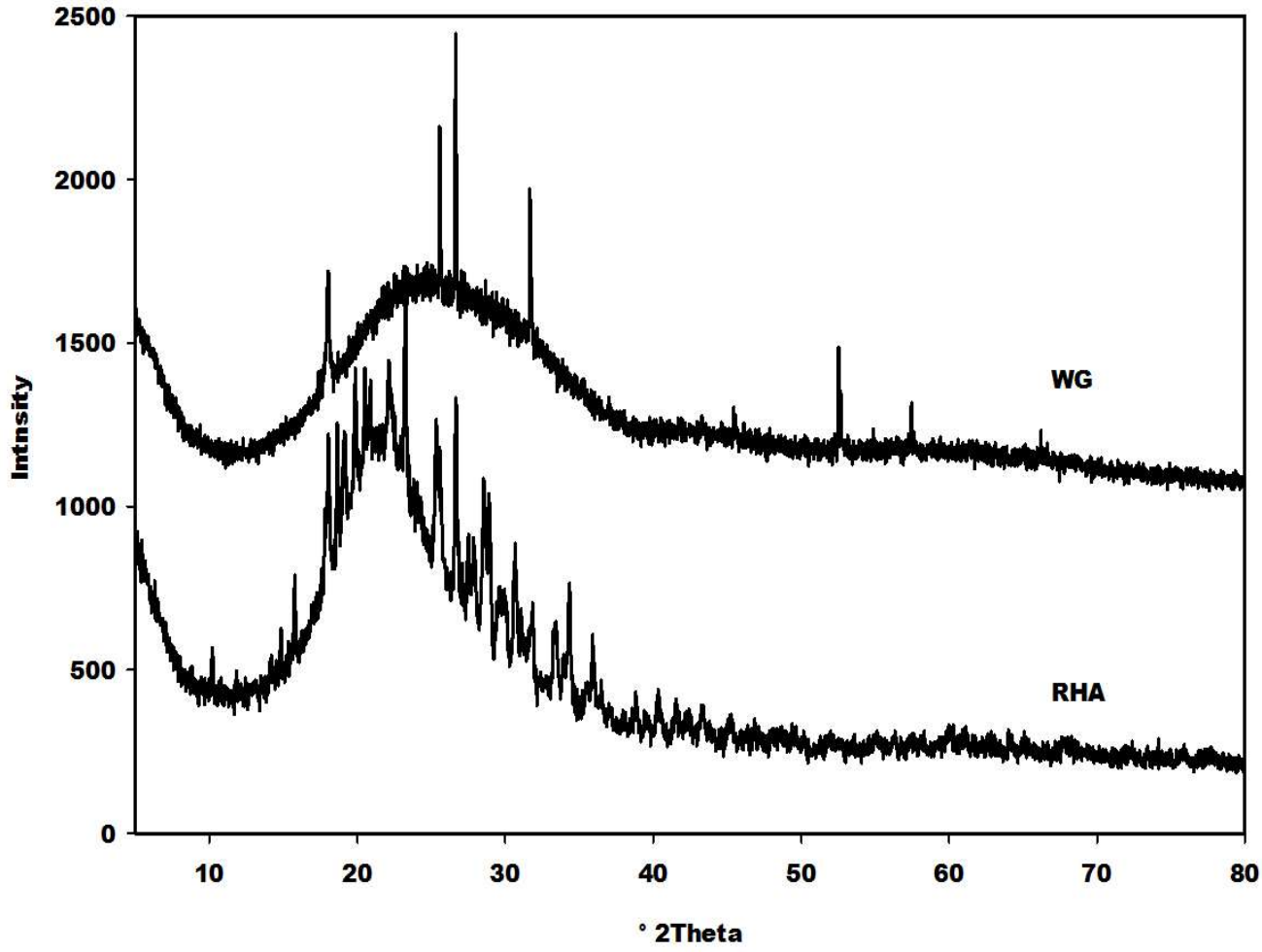

Fig. 2. XRD patterns of rice husk ash (RHA) and waste glass (WG).

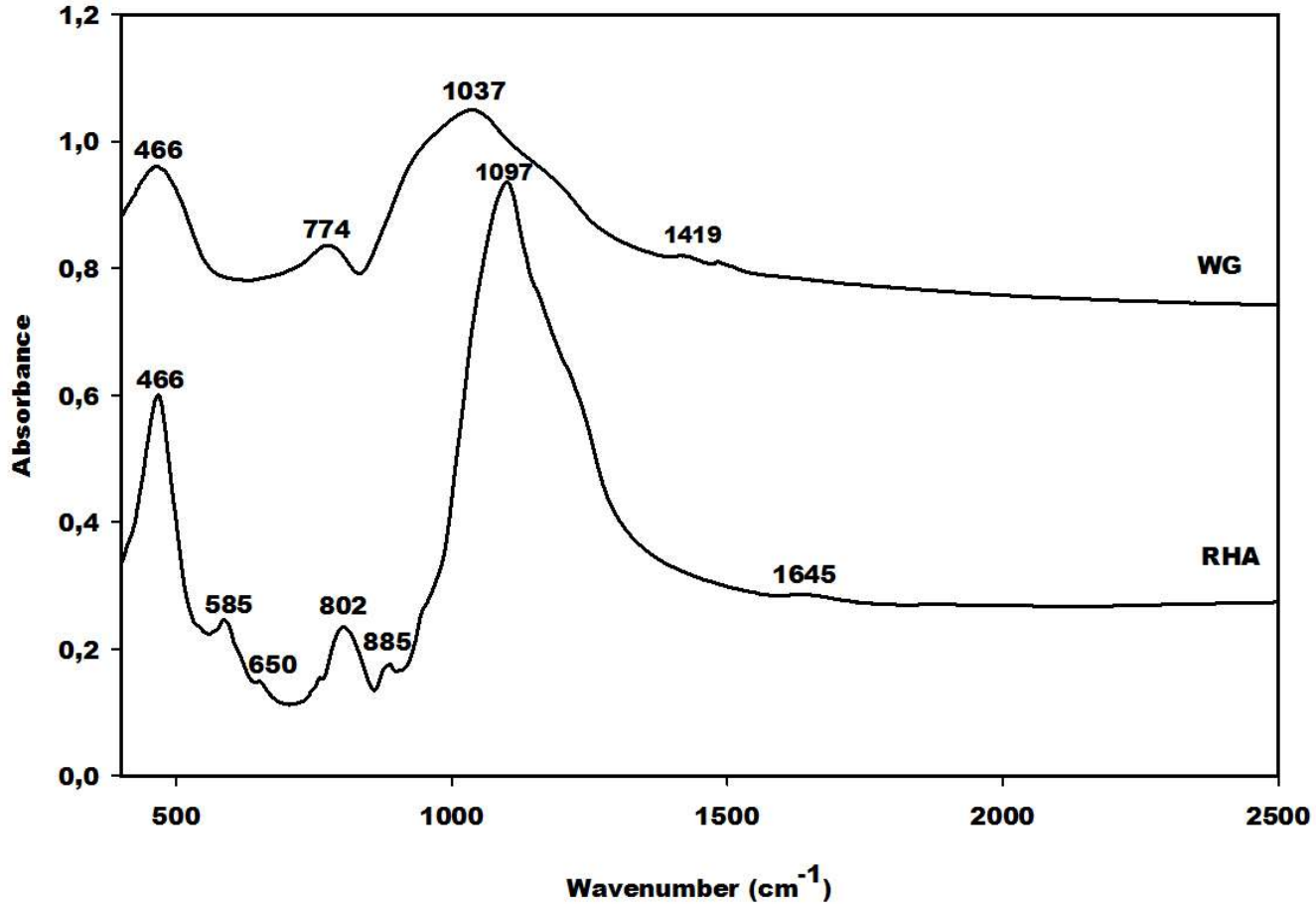

Fig.3. IR spectra of rice husk ash (RHA) and waste glass (WG).

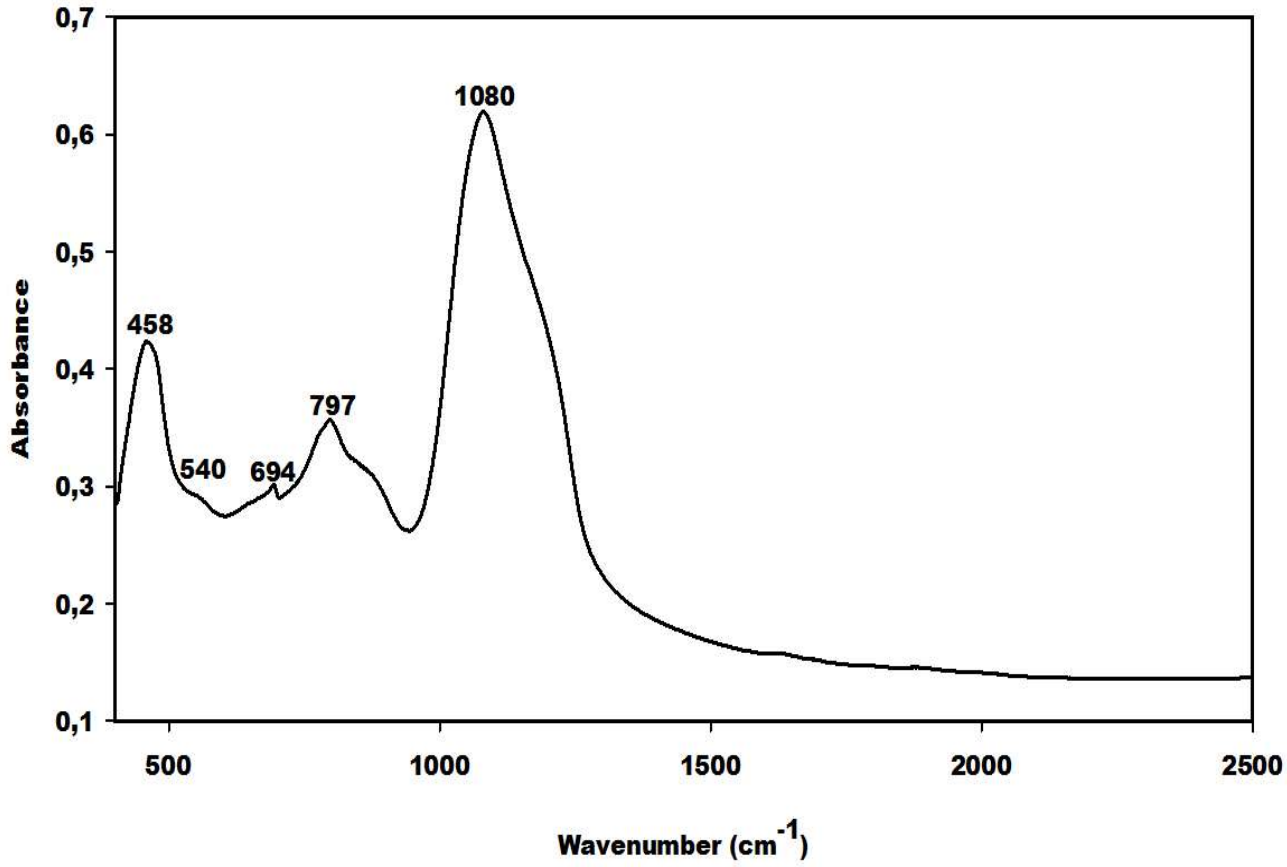

Fig.4. IR spectrum of metakaolin (MK).

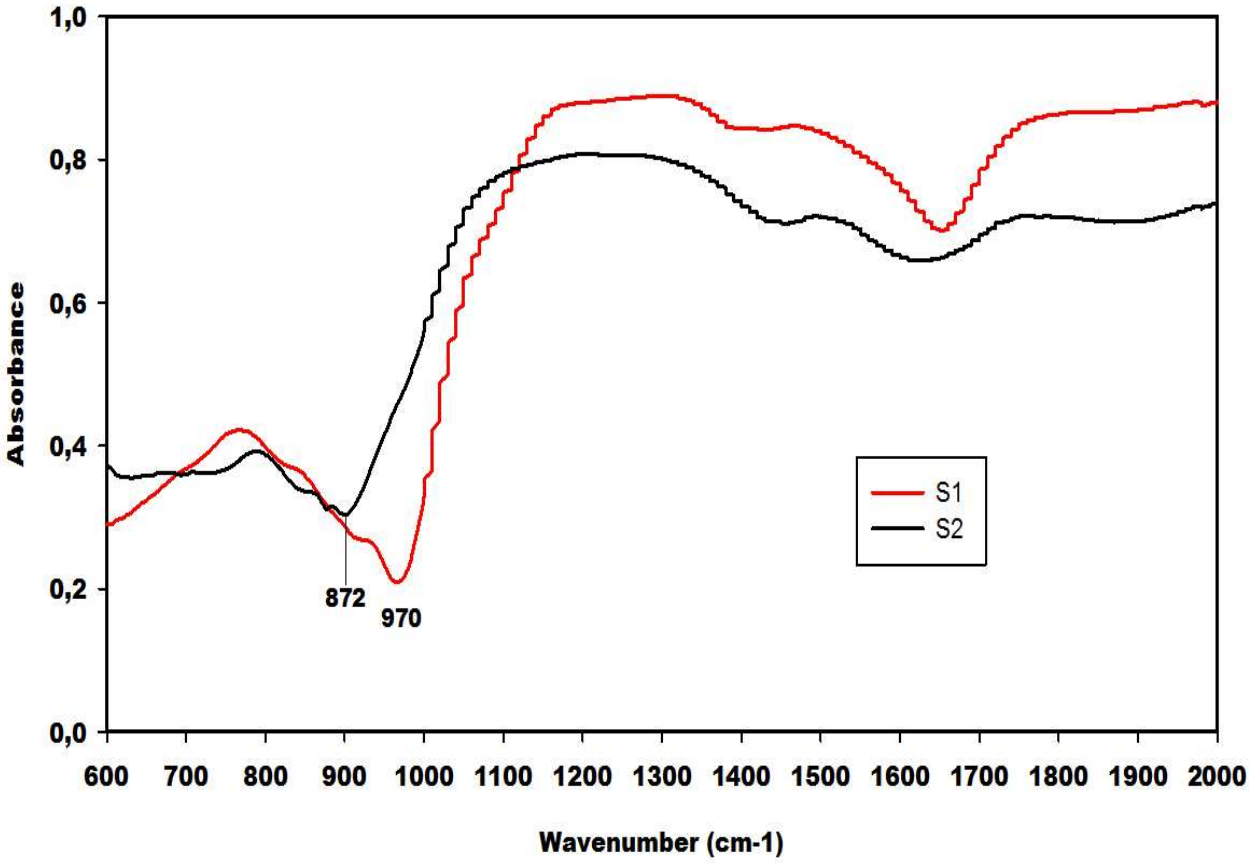

Fig. 5. ATR-IR spectra of sodium waterglass (S1 and S2).

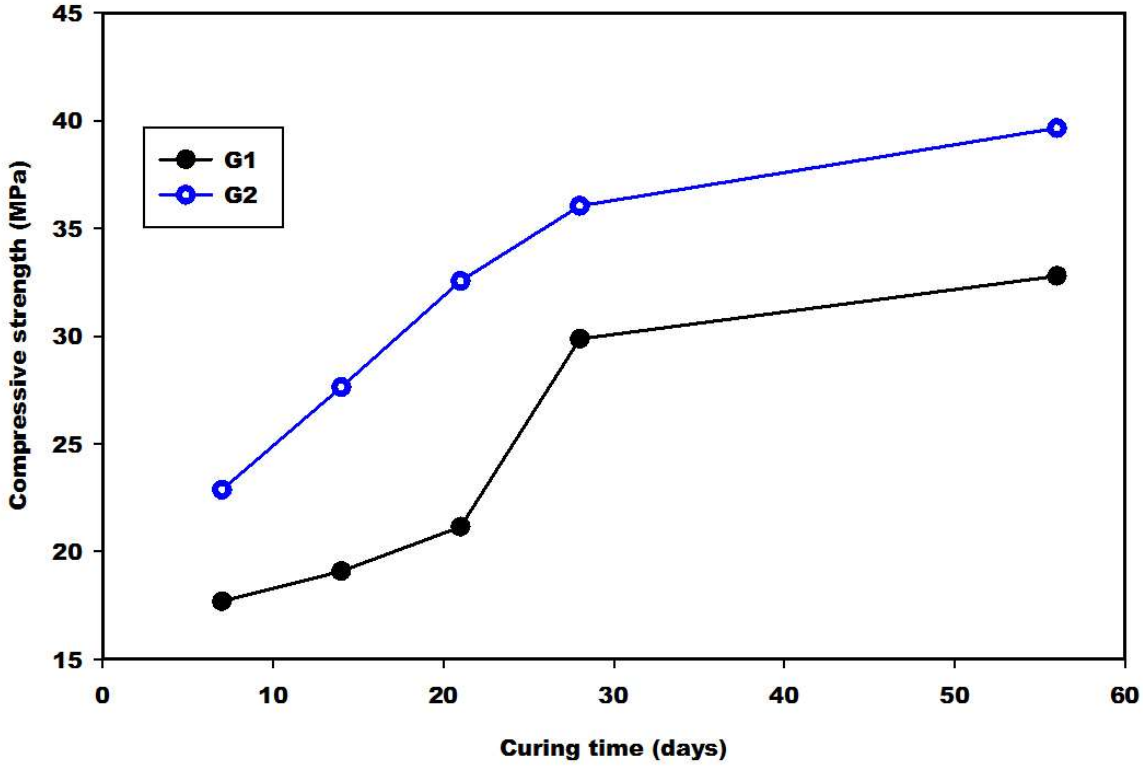

Fig. 6. Compressive strength of geopolymers G1 and G2 with various curing time.

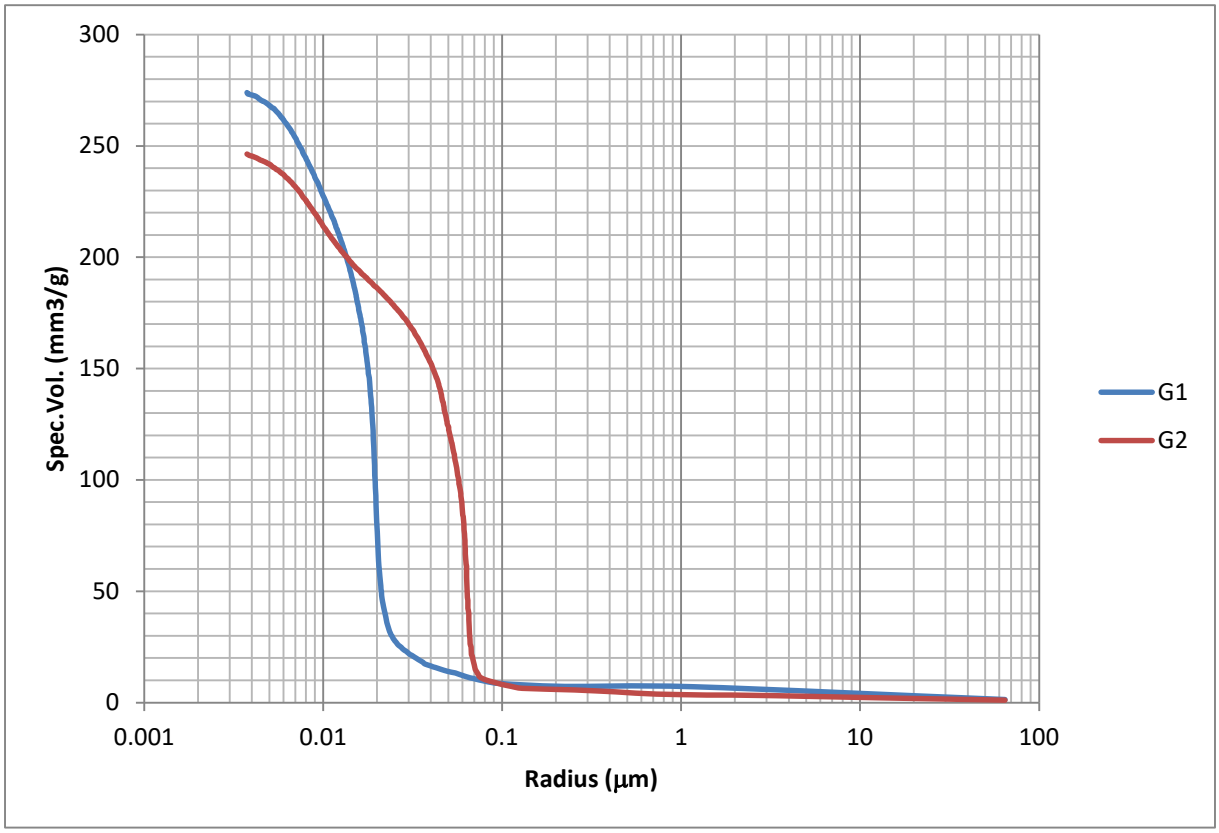

Fig. 8. Variation of cumulative pore volume of geopolymer cements G1 and G2.

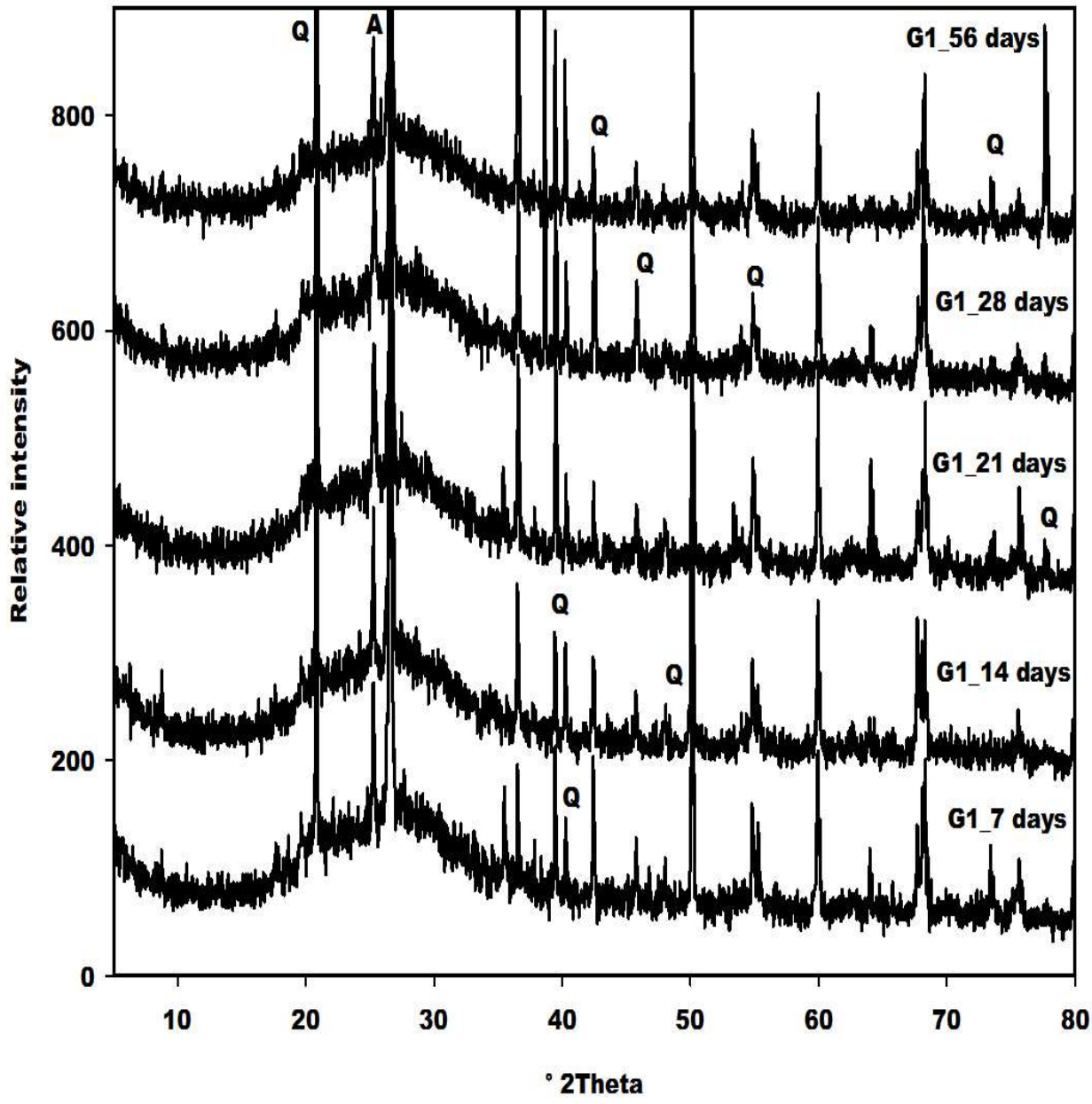

Fig. 9. X-ray patterns of geopolymers G1 with various curing time (I, A and Q denote peaks of Illite, Anatase and Quartz respectively).

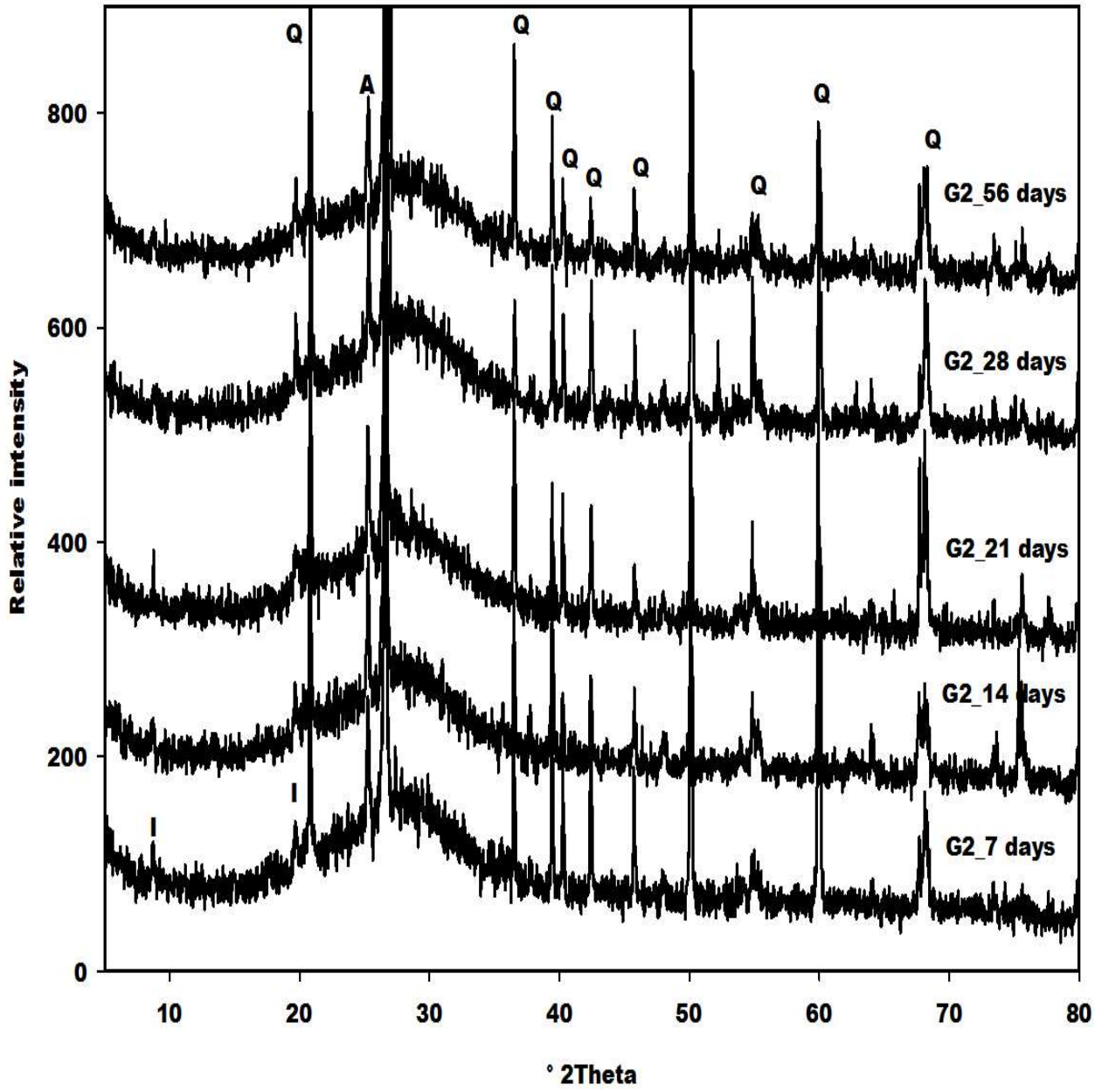

Fig. 10. X-ray patterns of geopolymers G2 with various curing time (I, A and Q denote peaks of Illite, Anatase and Quartz respectively).

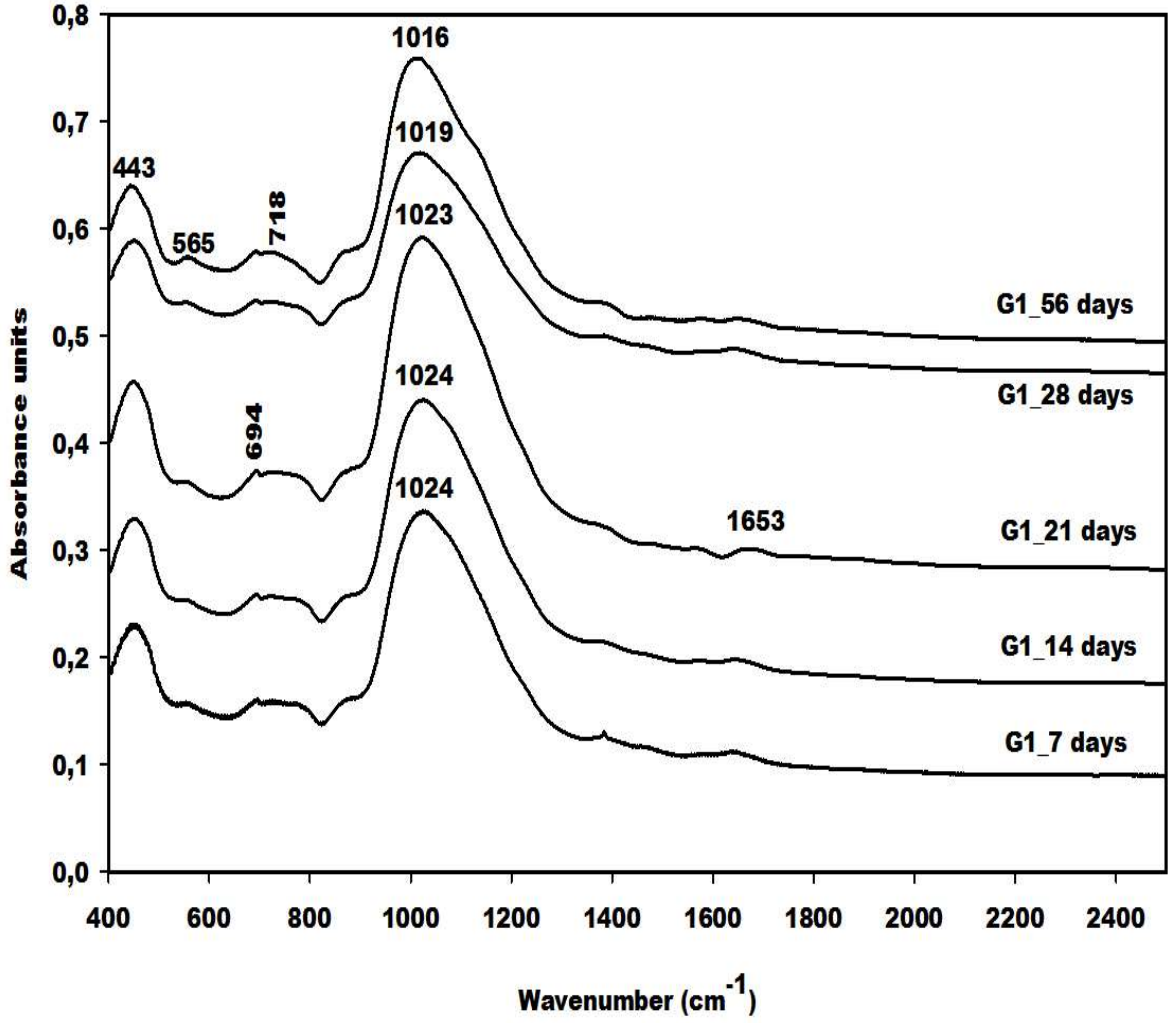

Fig. 11. IR spectra of geopolymers G1 with various curing time.

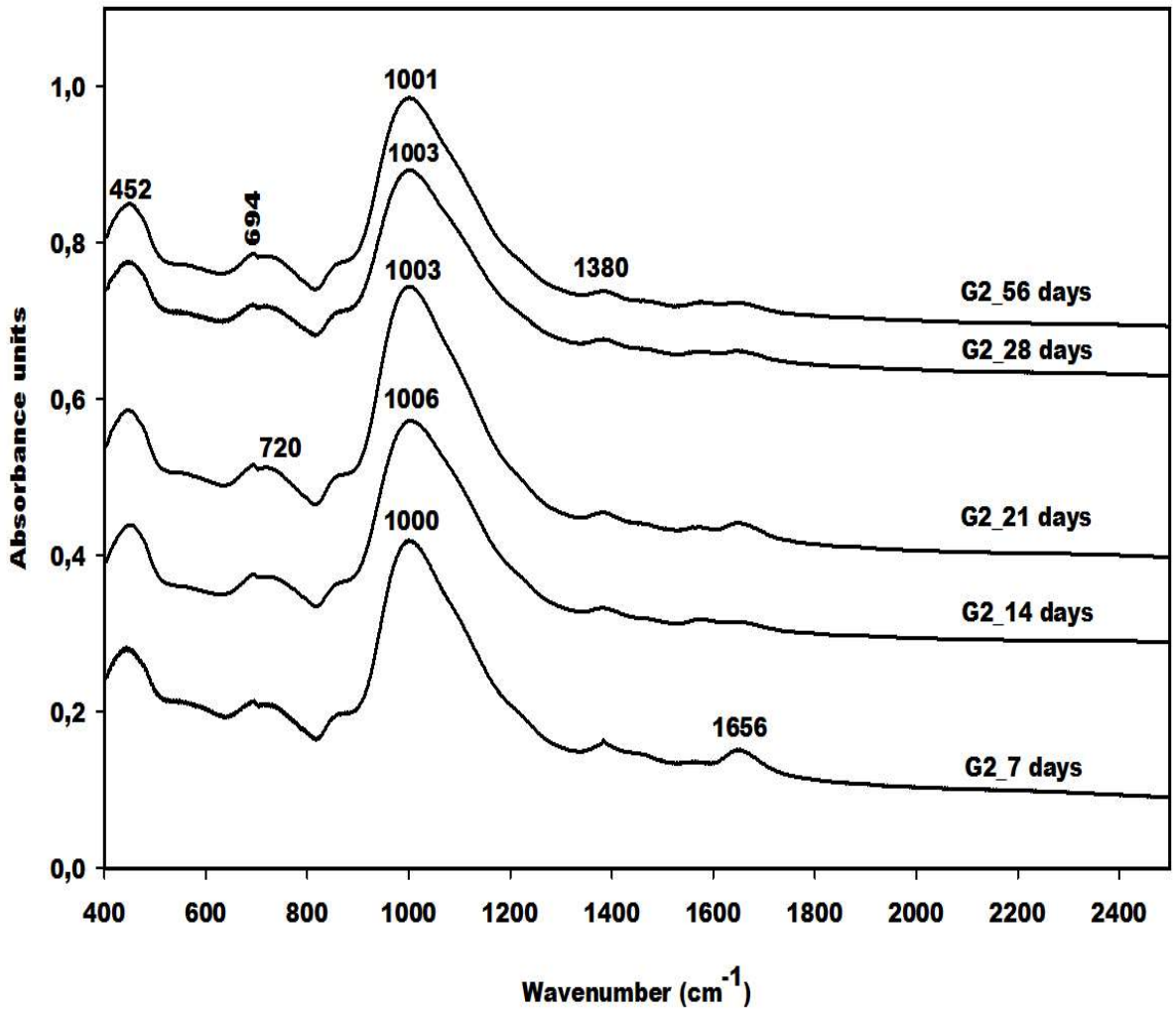

Fig. 12. IR spectra of geopolymers G2 with various curing time.

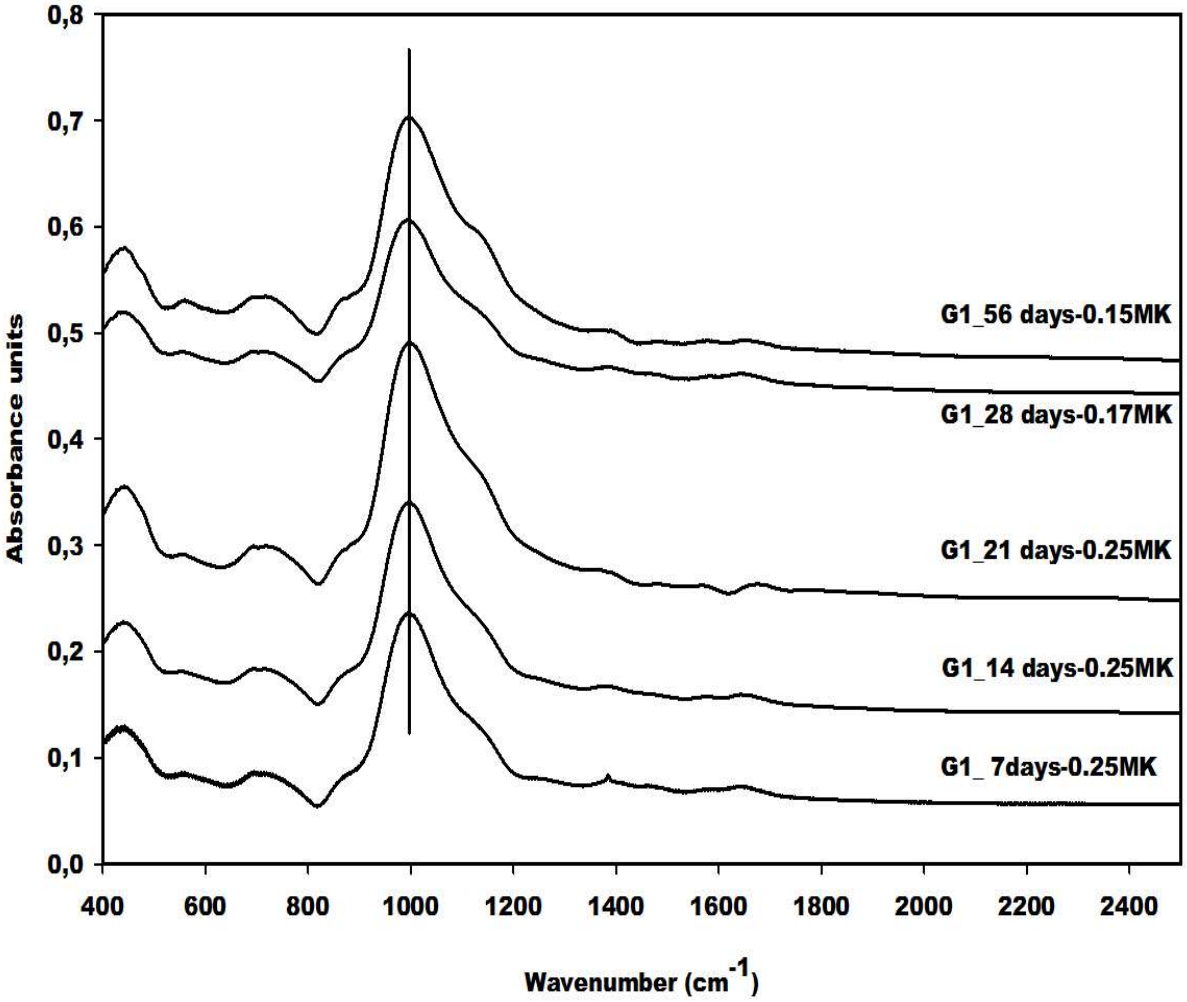

Fig. 13. Difference IR spectra of G1 with various curing time as denoted.

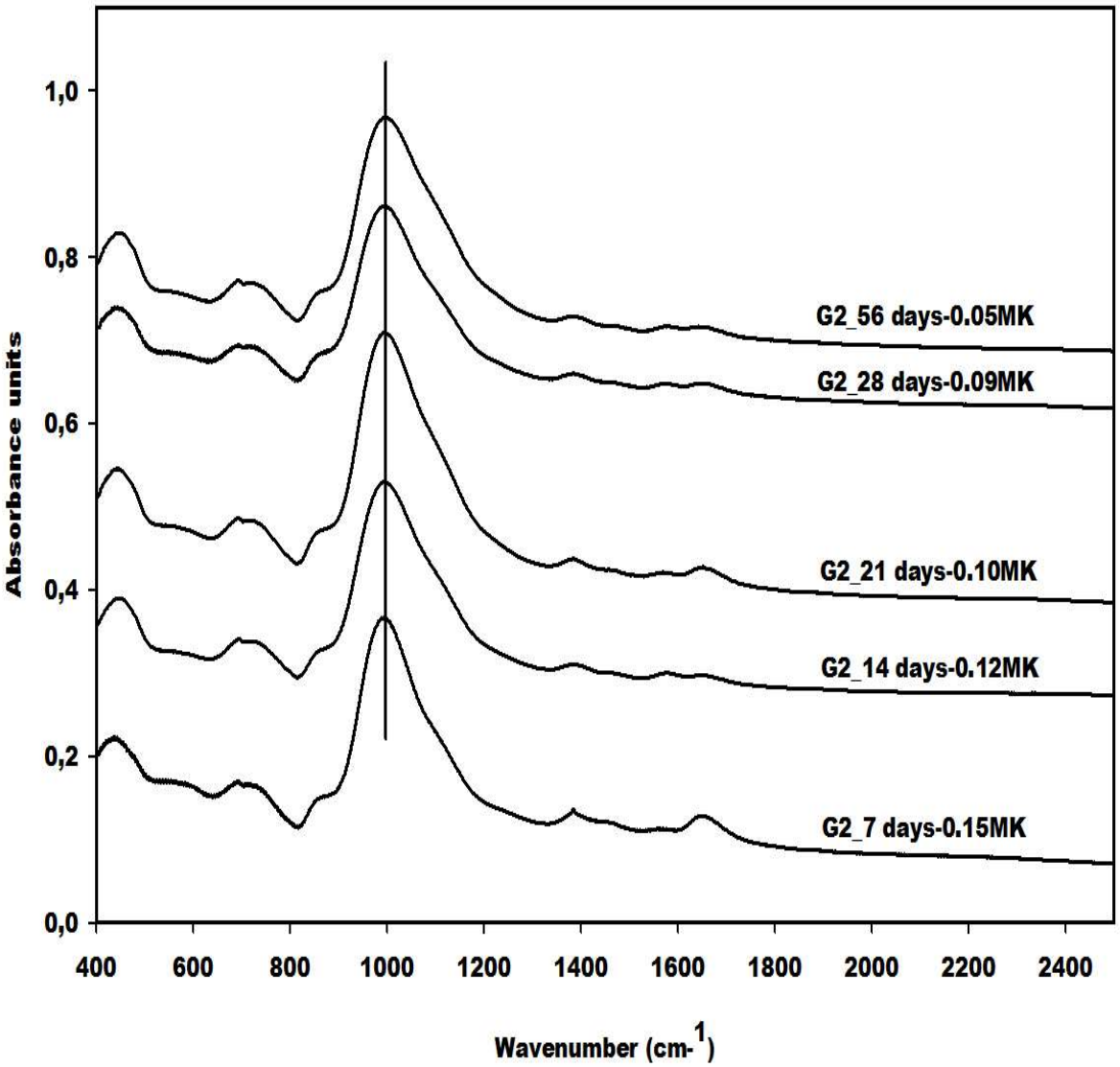

Fig. 14. Difference IR spectra of G2 with various curing time as denoted.

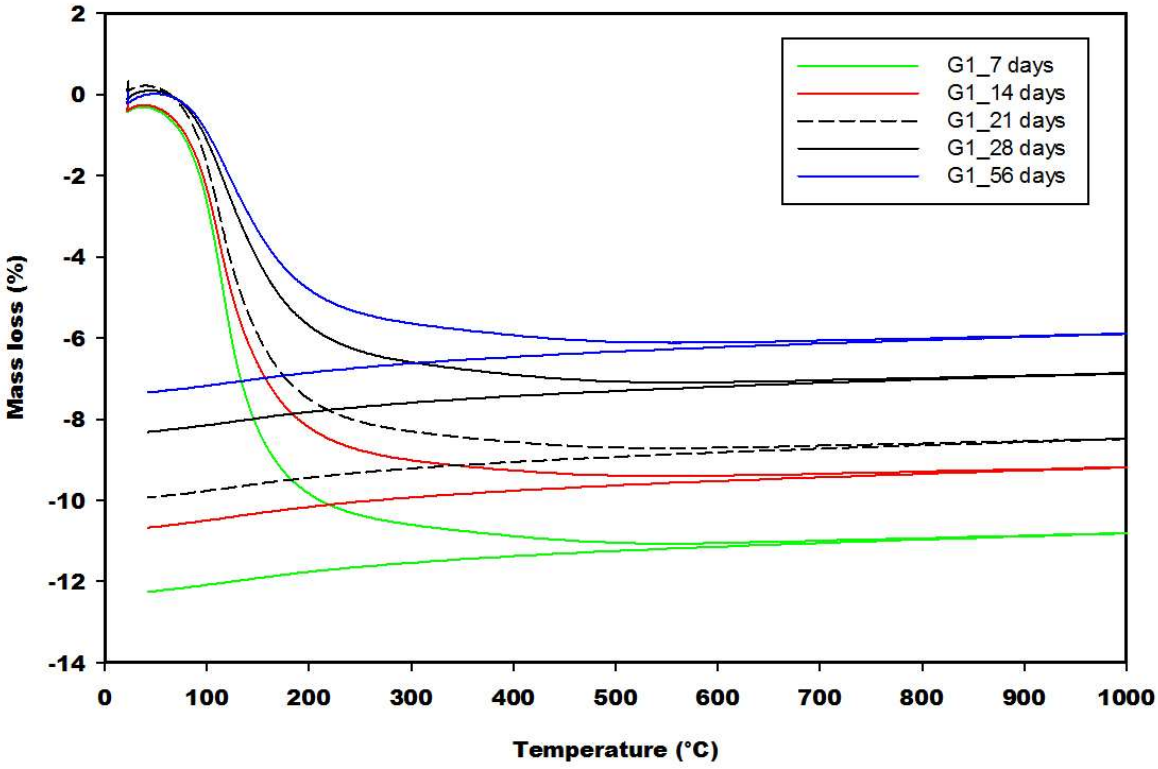

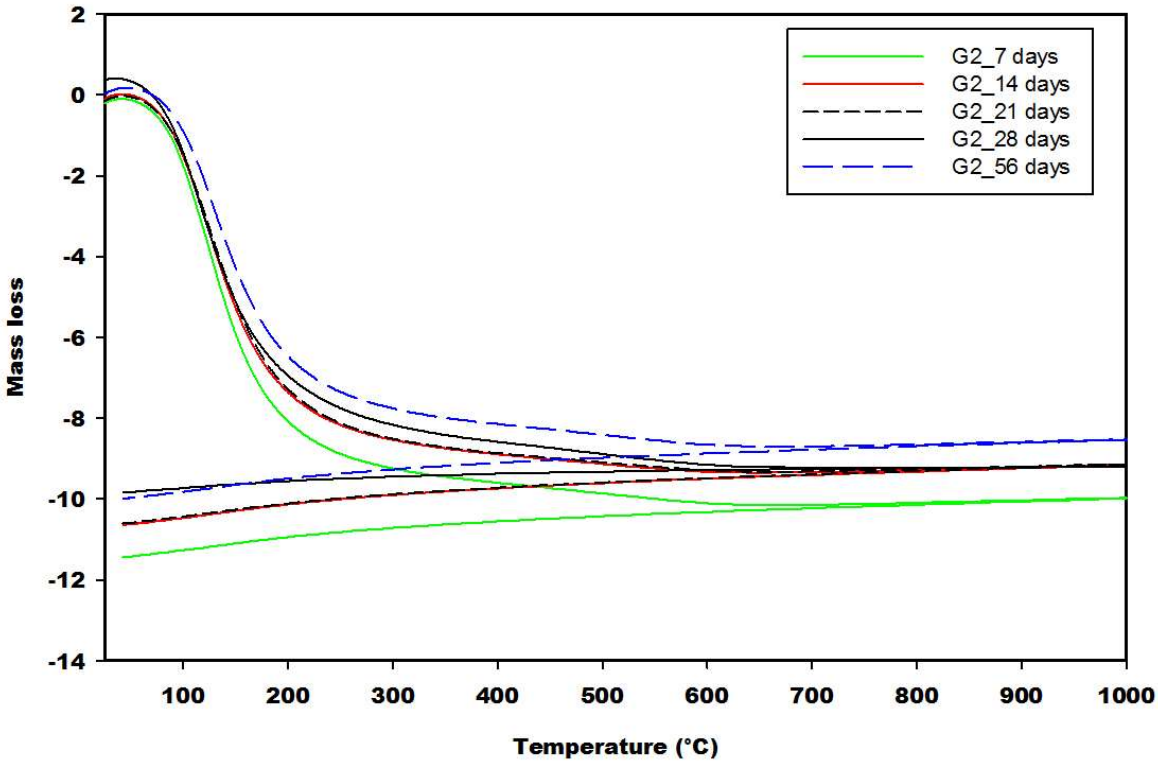

Fig. 15. TGA curves of geopolymer binders G1 and G2.

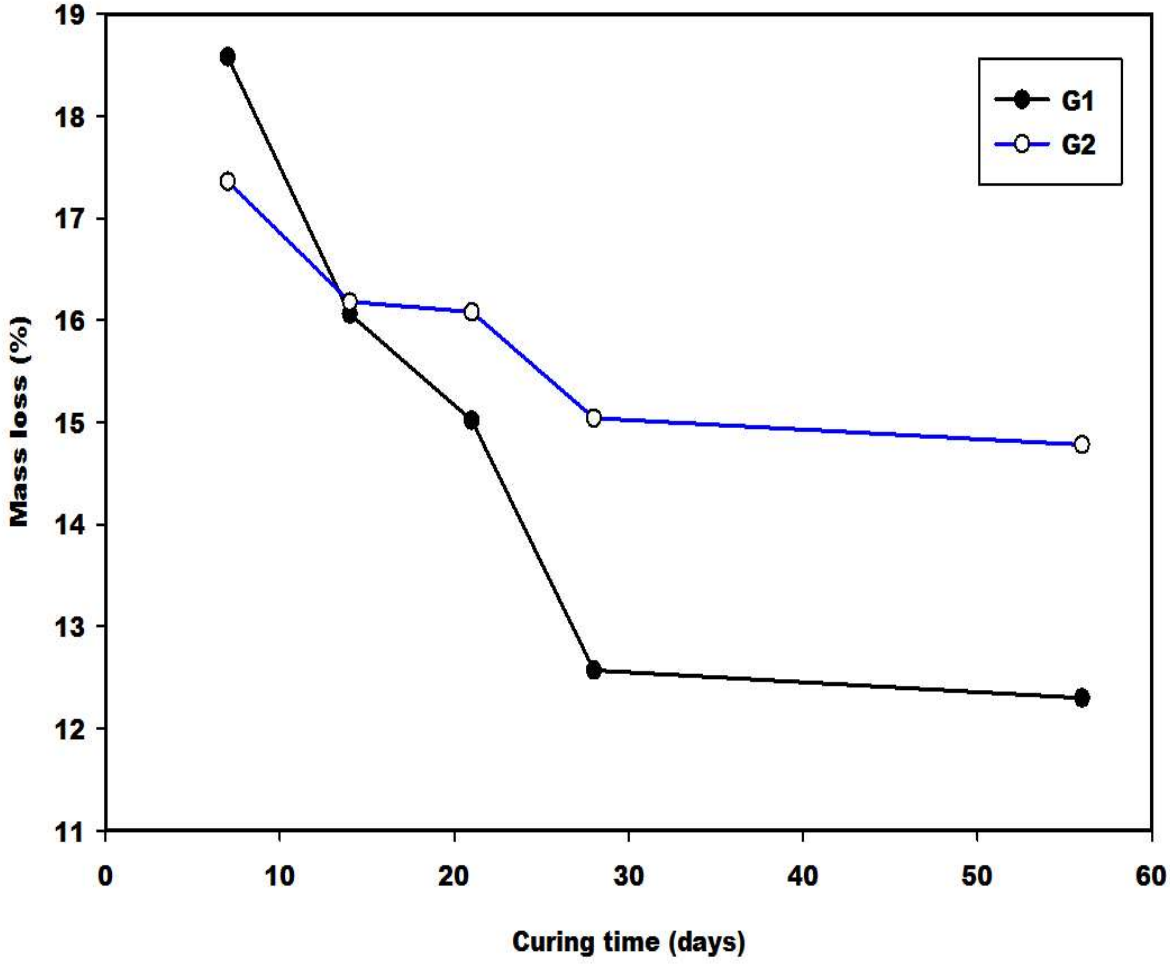

Fig. 16. Mass loss of geopolymers G1 and G2 with various curing time.